Effects of Pyrolysis Mode and Particle Size on the Microscopic Characteristics and Mercury Adsorption Characteristics of Biomass Char

Li Jia, Bao-guo Fan, Ben Li, Yu-Xing Yao, Rui-Peng Huo, Rui Zhao, Xiao-Lei Qiao, and Yan Jin *

Biomass chars (bio-chars) prepared under two pyrolysis modes and with four particle size ranges were investigated. The pyrolysis modes included isothermal pyrolysis and non-isothermal pyrolysis with three heating rates (5 °C/min, 10 °C/min, and 15 °C/min). The particle size ranges were 58-75 μm, 75-106 μm, 106-150 μm, and 150-270 μm. The pyrolysis characteristics, pore structures, surface morphologies, and functional groups of the bio-chars were characterized by TGA, specific surface area and porosity analyses, SEM, and FTIR. The mercury adsorption was further explored by the adsorption kinetics. The results established the optimum pyrolysis conditions for mercury adsorption: pyrolysis temperature of 600 °C, heating rate of 10 °C/min, and particle size of 58-75 μm. In addition, the mercury adsorption processes were affected by both physical adsorption and chemical adsorption. Furthermore, the rate constants of the pseudo-first-order and pseudo-second-order models gradually increased with decreasing particle size.

Keywords: Biomass char; Particle size; Isothermal; Non-isothermal; Mercury; Adsorption characteristics

*Contact information: College of Electrical and Power Engineering, Taiyuan University of Technology, Taiyuan, 030024, P. R. China; *Corresponding author: jinyan@tyut.edu.cn*

INTRODUCTION

At present, mercury is one of the most harmful trace elements, responsible for a large negative effect on the environment and on humans (Syversen and Kaur 2012). There are two major sources of mercury in the environment, namely natural and man-made; the latter accounts for one-third of the total mercury released into the environment. The annual mercury emissions in China are more than one fourth of the global amount (Zhang and Wong 2007). When coal is burned, the mercury contained in the coal is released into the environment, accounting for 50% of the total mercury emissions in China (Wu *et al*. 2011). China has required the mercury concentration limit in the flue gas of coal-fired power plants to be 30 μg/m^3 since January 1, 2015 (GB 13223-2011 2012).

Because of the special energy structure in China, the installed capacity of coal-fired power plants accounts for 69% of the total installed capacity in 2013. The coal consumed by power plants accounts for 60% of the total amount of coal produced. Due to China's large equipment capacity and its large amount of coal consumption, the pollutant emission is relatively concentrated in coal-fired power plants. Flue gas mercury removal technologies in coal-fired power plants aim to remove gaseous mercury. Currently, as there is no special mercury emission control equipment, research into mercury emission control in the flue gas from coal-fired power plants has mainly focused on three aspects: mercury removal before combustion, improvement of existing pollution control equipment, and

comprehensive emission control of pollutants (Gbor *et al*. 2006). According to the current circumstances, the method of adsorbent injection in combination with the existing typical air pollution control equipment, such as electrostatic precipitators (ESPs) and fabric filters (FFs), may become a promising technology for controlling mercury emissions in coal-fired flue gas (Zeng *et al*. 2004). Among these methods, activated carbon injection has been frequently applied, but many problems still exist with this technique (Carey *et al*. 1998; Graydon *et al*. 2009). Therefore, the development of efficient, low cost, and substitutable adsorbents is urgently needed.

Biomass char (bio-char) is a solid product obtained from the pyrolysis of biomass. It has complex pore structures and good surface characteristics. Much research into applying biomass to remove combustion pollutants has been conducted, including using the method of gas reburning after biomass gasification to control NO_X emissions in coal-fired boilers (Pisupati and Bhallaa 2008). The flue gas generated in coal-fired boilers can form high-temperature pyrolysis conditions, providing the energy necessary for the pyrolysis of biomass. The flue gas temperature changes with the flow, which forms non-isothermal pyrolysis conditions and a wide temperature range. Additionally, the particle size can affect the pyrolysis process. Therefore, studies on the effects of the pyrolysis mode and particle size on the mercury adsorption characteristics of bio-char are necessary for exploring low-cost mercury removal technologies and overcoming the disadvantages of the low calorific value and low utilization efficiency of biomass.

It has been found that the heating rate and particle size are the two main factors that affect the pyrolysis characteristics of biomass. These factors have important influences on the gas-solid heterogeneous reaction rate, and mainly affect heat and mass transfer in the chemical reaction process (Senneca 2007). Additionally, the production of gaseous products remarkably increases during biomass pyrolysis with an increase in the pyrolysis temperature (Becidan *et al*. 2007; Fu *et al*. 2011). There have been some studies on the elemental mercury adsorption characteristics of bio-chars (Fuente-Cuesta *et al*. 2012; Yin *et al*. 2012). Above all, the adsorption of mercury by bio-char is dependent upon the characteristics of the bio-char. However, the key points determined in the above studies were diverse. Some studies have been conducted on the effects of the preparation conditions on the pyrolysis characteristics of the resulting bio-char. However, there have been fewer studies on the effects of different heating rates and particle sizes on the pyrolysis characteristics and mercury adsorption properties of bio-char. Moreover, these effects change significantly with different kinds of pyrolysis materials. The conclusions drawn from these studies differ substantially due to lack of comprehensive analysis. In this study, a comprehensive study of the effects of different pyrolysis modes (isothermal and non-isothermal) and particle sizes on the mercury adsorption characteristics of bio-char, the microscopic characteristics of bio-char, and the adsorption kinetics was performed to systematically explore the corresponding reaction mechanism. The results provide a theoretical basis for the development of future mercury removal methods.

EXPERIMENTAL

Preparation and Characterization of the Samples

Walnut shell (WS) was selected as the raw material. The particle size was screened using a crusher and a vibrating machine following a quartering method to obtain WS biomass with four different particle size ranges, which were 150 μm to 270 μm (100 mesh),

106 μm to 150 μm (150 mesh), 75 μm to 106 μm (200 mesh), and 58 μm to 75 μm (250 mesh), labelled as A, B, C, and D, respectively. The pyrolysis modes included isothermal pyrolysis mode and non-isothermal pyrolysis mode. A vertical tubular furnace was selected for biomass pyrolysis. During the process of isothermal pyrolysis, when the furnace temperature reached the set temperatures (400 °C, 600 °C, 800 °C, and 1000 °C), the biomass was quickly sent into the furnace and pyrolyzed in a N_2 atmosphere for 10 min. The non-isothermal pyrolysis experiments were performed at three heating rates of 5 °C/min, 10 °C/min, and 15 °C/min to the final temperatures of 400 °C, 600 °C, 800 °C, and 1000 °C in a N_2 atmosphere. The biomass samples were also pyrolyzed for 10 min. After each pyrolysis experiment, the bio-char samples were kept in a desiccator until the material had cooled to the room temperature. The bio-chars obtained at 5 °C/min, 10 °C/min, and 15 °C/min heating rates were labelled as α, β, and γ. Compared with the non-isothermal preparation, the isothermal preparation was labelled as I.

The adsorption and desorption isotherms of the bio-char samples were obtained by performing N_2 adsorption and desorption experiments with an ASAP 2460 analyzer (Micromeritics, Norcross, GA, USA). The specific surface area was obtained from the Brunauer-Emmett-Teller (BET) equation, and the pore structure parameters of the samples were obtained by the Barrett-Joyner-Halenda (BJH) method. The moisture (M), volatile compound (V), ash (A), and fixed carbon (FC) contents were measured by a muffle furnace, in accordance with ASTM E1756-08 (2015). The reported value was the average value obtained from three parallel experiments. The functional groups on the surface of the bio-char were analyzed with a Vertex80V Fourier transform infrared (FTIR) spectrometer (Bruker, Madison, USA). The surface morphology of the bio-char was determined using a Nova Nano scanning electron microscope (SEM) 50 (Thermo Fisher Scientific, Hillsboro, USA). The pyrolysis characteristics of the biomass were determined by a TGA/SDTA851 thermogravimetric analyzer (Mettler Toledo, Zurich, Switzerland).

Fixed-bed Mercury Adsorption Experiments

In the fixed-bed mercury adsorption experiments, the fixed-bed experimental system was mainly composed of a Hg^0 permeator, a gas distribution system, a fixed-bed reactor, a continuous mercury vapor analyzer (VM3000, Mercury Instruments GmbH, Karlsfeld, Germany), and a tail gas absorption device. The Hg^0 concentration in the simulated flue gas at the outlet of the reactor was continuously measured by the VM3000 at a sampling interval of 1 s, and the amount of bio-char was 1 g. Before the experimental gas entered the VM3000, the $SnCl_2$ solution was used to reduce the Hg^{2+} (some Hg^0 oxidized on the surface of bio-char and escaped) in the experimental gas to Hg^0, and then into VM3000 with the original Hg^0 in the flue gas; thus the Hg^0 adsorption characteristics of the bio-char were obtained. The mercury vapor was produced within a mercury permeation tube, which was placed in a U-shaped borosilicate glass tube, and in order to ensure that the concentration of mercury in the inlet gas to the fixed bed was stable at 42 $\mu g/m^3$, the U-tube was maintained at 42 °C using a water bath. The total flow rate of the experimental gases was 1.4 L/min, which comprised the carrier gas and the equilibrium gas. The flow rate of N_2 carrying Hg^0 was 500 mL/min. The flow rate of the equilibrium gas (N_2) introduced at the entrance of the fixed-bed was 900 mL/min. The adsorption temperature was maintained at 50 °C. Before the adsorption experiment was carried out, the experimental gas was passed through the bypass to VM3000 for monitoring. After the Hg^0 concentration was stable for 30 min, the gas was passed into the fixed-bed reactor, and then the mercury concentration at the outlet was monitored online. In addition, in order to

prevent condensation of Hg^0 on the pipe wall due to low temperature, all pipings and tee joints were made of Teflon. The exhaust gas in the experiment process was treated by modified activated carbon. The mercury adsorption penetration coefficient, denoted η, and the total amount of mercury adsorbed per unit mass of bio-char, denoted q, were used to explore the mercury adsorption characteristics of bio-char. The parameter η is the ratio of the outlet Hg^0 concentration to the initial Hg^0 concentration in the flue gas at a certain time. In the same experimental conditions, the higher the η value is, the worse the corresponding mercury removal performance of the bio-char sample.

The parameter q represents the total amount of Hg^0 adsorbed by the bio-char from the beginning of the adsorption process and is calculated by Eq. 1 as follows:

$$q = \frac{F}{m}\int_0^t (C_{in} - C_{out}) \cdot dt \quad (1)$$

In this equation, C_{in} is the initial concentration of Hg^0 in the flue gas (ng/L), C_{out} is the corresponding concentration of Hg^0 at the outlet (ng/L), F is the flow rate of N_2 through the bio-char (L/s), m is the bio-char filling amount (g), q is the total amount of Hg^0 adsorbed per unit mass of bio-char (ng/g), and t is the adsorption time (s).

RESULTS AND DISCUSSION

Proximate and Ultimate Analyses

The results of the proximate and ultimate analyses of the biomass and bio-chars are shown in Table 1. It was found that the WS biomass had a higher content of volatile compounds on an air-dried basis, compared with the bio-chars. The devolatilization of volatile substances was beneficial to the formation of developed pore structures. The oxygen content was high, which indicated that oxygen-containing functional groups were abundant. During the pyrolysis of the biomass, the carbon-hydrogen bonds and carbon-oxygen bonds fractured, and hydrogen and oxygen elements were separated from the biomass, which resulted in a decrease in these element contents and an enrichment of carbon (Newalkar *et al*. 2014). Thus, the fixed carbon contents and gross calorific values of the bio-chars were higher. Additionally, the fixed carbon content was directly related to the pyrolysis temperature. Meanwhile, the contents of N and S in the biomass were relatively smaller, and during the process of pyrolysis, these were mainly in the form of small molecular compounds retained in the bio-char. The reduction degree of these was smaller than that of H and O, so the mass fractions of these increased. As the volatile compounds were sufficiently devolatilized under the isothermal pyrolysis mode, the volatile compound contents of the bio-chars were lower than the bio-chars prepared under the non-isothermal pyrolysis mode. With a decrease in the stationary temperature, the volatile compound contents steeply increased. The volatile compound content of the 400-D-I sorbent was 49.7%, which indicated that the devolatilization of the volatile compounds was not sufficient. Under the non-isothermal pyrolysis mode and with an increase in the heating rate, the volatile compound contents gradually increased. This result implied that more volatile compounds remained and less volatile compounds devolatilized; thus, the devolatilization degree of the volatile compounds gradually weakened. Meanwhile, with a decrease in the particle size, the influence of the heat and mass transfer decreased, which facilitated the pyrolysis process. As a result, volatile compound devolatilization was gradually enhanced.

Table 1. The Proximate and Ultimate Analyses of the Biomass and Bio-char

Sorbent	Proximate Analysis W_{ad} (%)				Ultimate Analysis W_{ad} (%)					Gross Calorific Value $Q_{ar,gr}$ (kJ/kg)
	V_{ad}	FC_{ad}	M_{ad}	A_{ad}	C	H	O	N	S	
WS-RAW	79.5	12.77	7.4	0.33	45.7	5.94	46.02	0.32	0.02	18435.17
600-D-I	18.66	75.84	0.79	4.71	86.32	1.15	4.92	1.18	0.08	29293.92
400-D-I	49.71	45.99	0.83	3.47	-	-	-	-	-	-
800-D-I	12.6	81.44	0.53	5.43	-	-	-	-	-	-
1000-D-I	9.65	83.94	0.52	5.89	-	-	-	-	-	-
600-D-α	20.16	74.33	0.52	4.99	-	-	-	-	-	-
600-D-β	20.35	74.59	0.73	4.33	-	-	-	-	-	-
600-D-γ	21.32	73.89	0.64	4.15	-	-	-	-	-	-
600-A-I	32.74	63.22	0.97	3.07	-	-	-	-	-	-
600-B-I	30.69	65.89	0.31	3.11	-	-	-	-	-	-
600-C-I	21.14	73.22	0.88	4.76	-	-	-	-	-	-

Note: W_{ad} is the mass fraction on air-dried basis.

Pyrolysis Characteristics of the Bio-char

The pyrolysis trend curves of the WS biomass under the different pyrolysis modes and with different particle sizes were similar and are shown in Fig. 1. The pyrolysis process of WS was consistent with that of cellulosic biomass (Sanchez-Silva *et al*. 2012). The main polymer components involved in the pyrolysis process were hemicellulose, cellulose, and lignin. Hemicellulose is mainly composed of glucose, mannose, xylose, and galactose. It has short molecular chains with saccharidic side-groups and an amorphous structure. It can be easily pyrolyzed over the low temperature range of 220 °C to 315 °C. Cellulose is a polymer with a straight chain formed by the polymerization of glucose molecules. It has a more stable structure. The pyrolysis temperature range of cellulose is higher than that of hemicellulose and is mainly from 315 °C to 400 °C. Lignin is formed by the polymerization of aromatic compounds without fixed shapes and forms a crosslinked network structure. The range of the chemical bond energy is very wide and difficult to decompose. The lignin pyrolysis process occurs over a wide temperature range from room temperature to 900 °C (Jia *et al*. 2018).

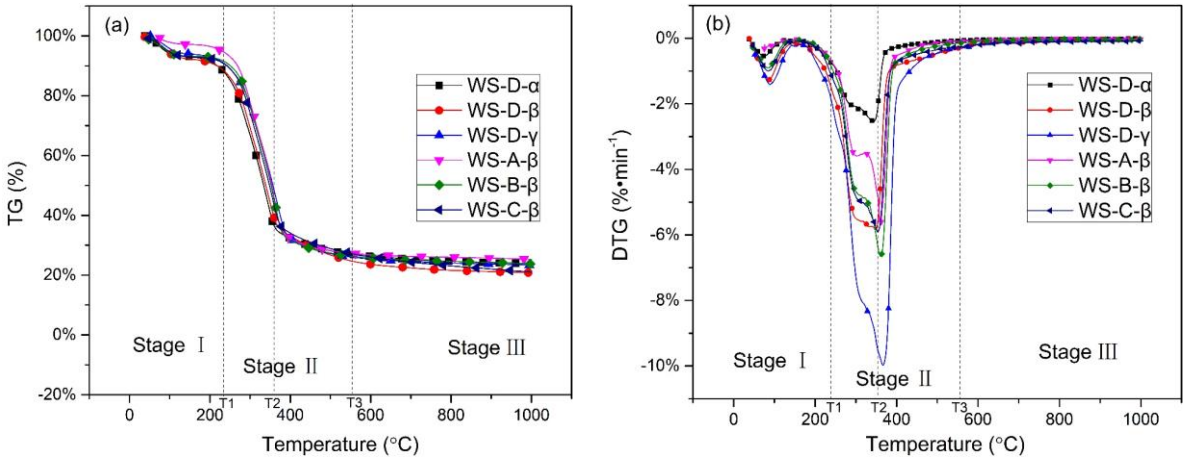

Fig. 1. The TG and DTG curves of WS in the different pyrolysis conditions: (a) TG curves; and (b) DTG curves

The pyrolysis process could be divided into three stages. The first stage occurred from room temperature to T_1 (the temperature corresponding to a weight loss ratio of approximately 10% was the initial devolatilization temperature of volatile matter (Duan *et al*. 2006)), which was approximately 200 to 250 °C. The main changes in the biomass in this pyrolysis stage occurred through dehydration, a small amount of internal depolymerization recombination, and the "glass transition phenomenon" (Antal and Varhegyi 1995). The preparatory work for the next stage of the rapid pyrolysis of biomass was also accomplished. The second stage occurred from T_1 to T_3, where T_3 was in the range of 300 to 500 °C. This stage accounted for the main weight loss in the pyrolysis process. Most of the organic components decomposed rapidly, and pyrolysis products were formed. A strong weight loss peak appeared at approximately 360 °C, which was mainly due to pyrolysis of cellulose. Meanwhile, a unique shoulder peak appeared at approximately 310 °C before the strong weight loss peak and was mainly due to the pyrolysis of hemicellulose. The third stage of pyrolysis occurred from T_3 to the final temperature and exhibited only a slight weight loss. In this stage, slow pyrolysis of the carbonaceous materials in the solid residues principally occurred to form the final bio-char.

According to the pyrolysis curves and related pyrolysis characteristic parameters, a comprehensive index of the pyrolysis characteristics (D) was proposed to characterize the degree of difficulty for the devolatilization of biomass volatile compounds, which was calculated by Eq. 2. The larger the value, the more likely pyrolysis behavior will occur. The related characteristic pyrolysis parameters are shown in Table 2.

$$D = \frac{(dw/dt)_{\max} \cdot (dw/dt)_{\text{mean}} \cdot V}{T_1 \cdot T_2 \cdot \Delta T_{1/2}} \quad (2)$$

where T_2 is the temperature corresponding to the maximum devolatilization rate of volatile in the second stage of pyrolysis (°C), $(dw/dt)_{\max}$ is the maximum weight loss rate during pyrolysis, which is the peak value of DTG (%/min), $(dw/dt)_{\text{mean}}$ is the average weight loss rate in the second and third stages of pyrolysis (%/min), V is the total amount of volatile compound devolatilization in the second stage of pyrolysis (%), and $\Delta T_{(1/2)}$ is the temperature (°C) corresponding to a $(dw/dt)/(dw/dt)_{\max}$ of 1/2.

Table 2. Biomass Pyrolysis Characteristic Parameters

Sorbent	T_1 (°C)	T_2 (°C)	T_3 (°C)	$(dw/dt)_{\max}$ (%/min)	V (%)	$(dw/dt)_{\text{mean}}$ (%/min)	$\Delta T_{(1/2)}$ (°C)	D
WS-A-β	264	359	498	-5.69	62.82	-0.89	282	1.19E-11
WS-B-β	243	360	505	-6.65	63.73	-0.89	280	1.54E-11
WS-C-β	231	353	532	-5.90	63.93	-0.92	274	1.55E-11
WS-D-β	202	349	550	-5.84	66.18	-0.88	267	1.81E-11
WS-D-α	200	344	494	-2.53	63.16	-0.42	260	3.80E-12
WS-D-γ	224	366	571	-9.97	65.97	-1.33	283	3.76E-11

In the case of certain particle sizes, the T_1, T_2, T_3, and D all increased with the increase in the heating rate. The thermogravimetric (TG) curve moved to the high-temperature zone and the peak value interval of the DTG curve broadened, accompanied with the hysteresis phenomenon. The formation of the temperature gradient was intensified with an increase in the heating rate because of the poor thermal conductivity of the biomass, which inhibited the process of heating and decomposition of the internal particles (Ma *et al*. 2015). Meanwhile, the amount of volatile compound devolatilization initially increased

and then decreased with an increase in the heating rate. The amount of devolatilization was the highest when the heating rate was 10 °C/min. The reason for this was that, while increasing the heating rate could accelerate the devolatilization of the volatile compounds, the reaction rate between the free radicals that were produced during pyrolysis and the intrinsic hydrogen was lower than the rate of free radical formation, which led to the combination of free radicals and the formation of a high polymer that was difficult to devolatilize. This was adverse to the devolatilization of volatile compounds.

Furthermore, for certain heating rates, the biomass exhibited a similar weight loss trend, with a decrease in particle sizes. However, the T_3 decreased gradually, and the reaction region became narrow with an increase in the particle size, which was because of the great influence the particle size had on the process of heat and mass transfer. With a decrease in the particle size, it was easier to transfer heat and the temperature difference between the particles and the external decreased. Also, the gas produced during pyrolysis could discharge without delay. While the internal structure of the biomass particle was porous, if the volatile compounds devolatilized during the first-order cracking reaction did not discharge quickly, the second-order cracking reaction would occur with the formation of some condensable gases during the process of outward release from the intra-particle structure, which is not conducive to the generation of volatile compounds. Moreover, according to the D values, it was found that the heating rate played a more important role in the pyrolysis of the biomass than the particle size, in the conditions analyzed.

Pore Structures of the Bio-chars

The pore structures of the bio-char were characterized, and the results are shown in Table 3. The differential and accumulated pore volumes of the bio-chars are shown in Fig. 2. In this paper, the specific surface area per unit volume, Z, was introduced to characterize the pore richness and study the influence of the pore structure on the mercury adsorption capacity of the bio-char. This parameter was calculated by Eq. 3 as follows,

$$Z = S_0 / V_0 \quad (3)$$

where S_0 is the BET specific surface area of the bio-char (m^2/g) and V_0 is the accumulated pore volume of the bio-char (cm^3/g).

The surface fractal dimension (D_S) was another important parameter for describing the pore structure of the bio-char and could be obtained from Eq. 4 (Pfeifer 1988; Jarzbski *et al*. 1995):

$$\ln(V/V_m) = (D_S - 3) \cdot \ln(\ln(p_0/p)) + C \quad (4)$$

where V/V_m is the relative amount of adsorption, D_S is the fractal dimension, p_0/p is the reciprocal of the relative pressure, and C is a constant.

In the case of a certain particle size and with an increase in the pyrolysis temperature, the BET specific surface area, accumulated pore volume, D_S, and Z of the bio-char all initially increased and then decreased. The specific surface area and pore volume of the 600-D-I sorbent were the highest among all the samples. In contrast, the pore structure parameters of the 400-D-I sorbent were the lowest. As was mentioned above, the pyrolysis extent of the biomass and devolatilization of the volatile compounds were not sufficient at 400 °C, which resulted in pore structures that were not perfectly formed and contained mainly macroporous structures. Additionally, the Z and D_S were lower, and the surface structure of the sorbent was comparatively well ordered. As the further devolatilization of volatiles was promoted at 600 °C, the formation of new pores was

simultaneously promoted. A large number of mesopores were generated in the bio-char. The specific surface area and pore volume increased substantially, the D_S was higher, the surface structure was disordered, the pores formed were deeper, and the Z was higher. These results indicated that the pore structures were well developed, which was beneficial to the adsorption of mercury (Fan *et al*. 2016). A further increase in the pyrolysis temperature led to a collapse of the pore structure and a flattening of the bio-char surface due to the structure changes of the silicate caused by high temperatures (Keown *et al*. 2008; Park *et al*. 2010), which resulted in a decrease in the D_S. Furthermore, when the pyrolysis temperature was in the range of 600 °C to 850 °C, some of the volatile compounds were involved in a second-order cracking reaction, which formed tar. As these volatile compounds were from the deeper inner part of the biomass particle, the tar produced, which was in a semi-devolatilization state, was able to block the pore structure (Babu and Sheth 2006). Thus, the specific surface area and pore volume of the 800-D-I sorbent decreased significantly. Nevertheless, when the temperature was increased to 1000 °C, the coalescence of small pores occurred, which led to a further decrease in the pore richness. Meanwhile, the tar residue in the pores devolatilized, which was accompanied by the devolatilization of lighter volatile compounds, such as H_2. As a result, the specific surface area and pore volume were slightly higher than those of the sorbents obtained at 800 °C, and the pore structure tended to develop into macropores.

Compared with the pyrolysis temperature, the influence of the heating rate on the pore structures was lower. With an increase in the heating rate, the biomass underwent a wider temperature region of the pyrolysis process. And considering that the pyrolysis temperature and the devolatilization rate of volatile compounds were positively correlated, the devolatilization rate was gradually increased. Additionally, the pyrolysis products need abundant time to diffuse from the intra-particle structure in an orderly manner. Otherwise, these products could accumulate inside the particles, which would result in the obstruction of pore structures. Thus, an increase in the heating rate was beneficial for the development of the pore structure, and the pore richness increased gradually. In addition, in the low-temperature region, lower pyrolysis temperatures resulted in slower devolatilization rates, which was beneficial for the retention of the pore structure. Since the heating rates of 600-D-β and 600-D-γ sorbents were higher, the pyrolysis process mainly occurred in the low-temperature region; the specific surface area and pore volume of these sorbents were higher.

The pyrolysis process of the 600-D-α sorbent mainly occurred over the range of 550 °C to 600 °C, and so the relative pore volume of the macropores was higher. Also, the D_S was lower, which indicated that the surface structure was smooth and regular. The pores that formed were shallower, which was unfavorable for the adsorption of mercury. Similarly, compared with the 600-D-α, 600-D-β, and 600-D-γ sorbents that were prepared under the non-isothermal pyrolysis mode, the BET specific surface area and accumulated pore volume of the 600-D-I sorbent were lower.

The pore structure parameters of the bio-chars generated by pyrolysis increased gradually with decreasing particle size. As mentioned above, on the one hand, the amount of volatiles devolatilized in the pyrolysis process increased, which facilitated the development of the pore structure. On the other hand, due to the effect of shear stress during the process of biomass crushing, the particle size decreased, which was accompanied by a gradual increase in the specific surface area, most probable pore size, Z, and D_S of the bio-chars.

The 600-D-I sorbent had the highest most probable pore size, which meant a decreased resistance of mercury entering the inner particle, so the sorbent had the highest absorption ability. Meanwhile, it was found that the pyrolysis temperature and particle size were more influential on the pore structure of the bio-char than the heating rate.

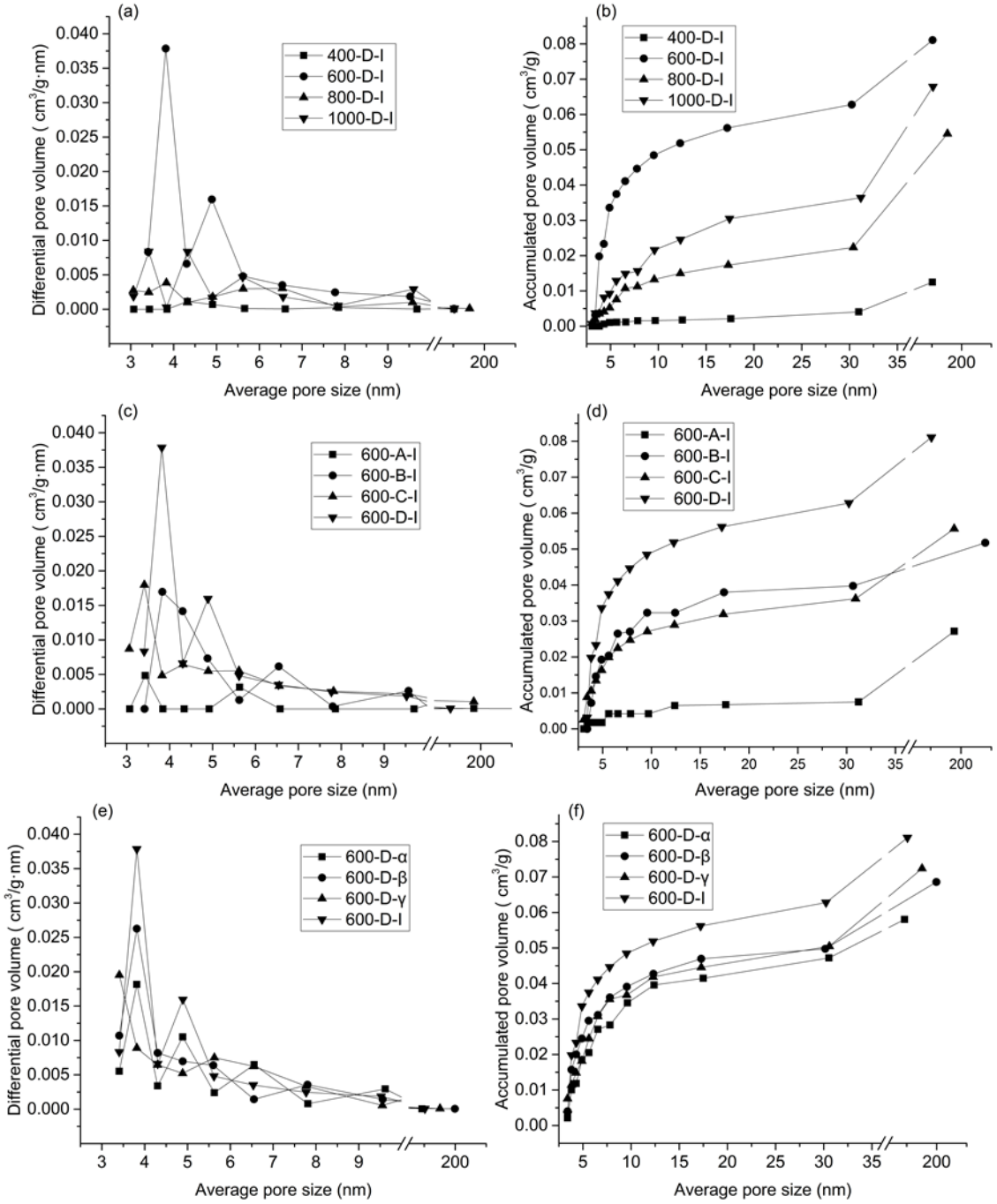

Fig. 2. Differential and accumulated pore volumes of the bio-chars prepared under different pyrolysis modes and with different particle sizes: (a) and (b) different temperatures; (c) and (d) different particle sizes; (e) and (f) different heating rates

It could be seen from the accumulated pore volume curves of the bio-chars that when the pore size was above 35 nm, the accumulated pore volume increased slowly, which indicated that macropores made a smaller contribution to the pore volume of the bio-char. The pore volume mainly consisted of mesopores. Meanwhile, it was concluded that there was a positive correlation between the mercury adsorption capacity of the bio-char and the accumulated pore volume.

Table 3. Pore Structure Parameters of the Bio-chars Prepared under Different Pyrolysis Modes and with Different Particle Sizes

Sorbent	BET Specific Surface Area (m^2/g)	Accumulated Pore Volume (cm^3/g)	Most probable pore size (nm)	D_S	Z	Relative Specific Pore Volume (%)	
						Micropores and Mesopores	Macropores
400-D-I	2.575	0.012	2.3804	2.5325	214	29.91	70.09
600-D-I	150.261	0.081	4.0614	2.7219	1855	77.44	22.56
800-D-I	45.396	0.055	2.5471	2.5101	825	46.27	53.73
1000-D-I	54.228	0.068	2.5331	2.5311	797	41.43	58.57
600-D-α	215.714	0.156	2.6649	2.7622	1383	79.74	20.26
600-D-β	280.762	0.179	2.7845	2.8526	1562	80.57	19.43
600-D-γ	287.792	0.182	2.9954	2.8353	1585	81.31	18.69
600-A-I	14.815	0.027	2.4727	2.6698	548	27.74	72.26
600-B-I	83.987	0.052	3.3125	2.7695	1615	64.62	35.38
600-C-I	109.149	0.062	3.8682	2.7129	1760	76.43	23.57

Surface Chemical Properties of the Bio-chars

In the research on the surface functional groups of bio-char, the relative contents of the functional groups were characterized by fitting the resolved peak areas (Ibarra *et al*. 1996; Koch *et al*. 1998). The infrared spectrum of bio-char could be divided into four main regions: the hydroxyl vibration zone (3600 to 3000 cm^{-1}), the aliphatic-CH vibration zone (3000 to 2700 cm^{-1}), the oxygen-containing functional group vibration zone (1800 to 1000 cm^{-1}), and the aromatic-CH out-of-plane vibration zone (900 to 700 cm^{-1}), which are denoted zones a, b, c, and d, respectively. Among the functional groups, hydroxyl and oxygen-containing functional groups including COOH and C=O were the main factors affecting the mercury adsorption of bio-char, as they could increase the adsorption energy of mercury on the surface of the bio-char (Zhang *et al*. 2015). The infrared spectra of the bio-chars are shown in Fig. 3, and the relevant parameters obtained by fitting are shown in Table 4.

The energy of the hydrogen bonds formed by hydrogen and oxygen was stronger, which resulted in a broad wave-crest belt in the hydroxyl vibration zone. This mainly involved free hydroxyl groups, which implied that the -OH functional groups of the biomass were cleaved during pyrolysis, with an increase in the pyrolysis temperature. This reaction produced moisture and also had an inhibitory effect on the production of phenols and alcohols (Keown *et al*. 2007).

The aliphatic-CH vibration zone mainly consisted of the stretching vibrations of the aliphatic compounds $-CH_2$ and $-CH_3$. The cleavage of alkyl side chains was promoted with increasing pyrolysis temperature, due to a large amount of CH_4 and other gases devolatilization, which resulted in a drastic decrease in the corresponding contents of these functional groups. When the temperature increased to 800 °C and 1000 °C, the relevant functional groups disappeared.

Table 4. Fitting Results of the Bio-chars Produced under Different Pyrolysis Modes and with Different Particle Sizes

Sorbent	A zone	B zone	C zone	D zone	C-O Functional Group	C=C Functional Group	COOH and C=O Functional Groups
400-D-I	33	83	2979	184	1019	855	332
600-D-I	28	6	2170	85	733	788	127
800-D-I	11	0	139	12	53	44	10
1000-D-I	12	0	40	0	0	26	0
600-D-α	15	2	976	94	355	403	28
600-D-β	20	2	1288	110	464	532	40
600-D-γ	15	0	1183	105	435	437	56
600-A-I	0	3	76	5	27	12	3
600-B-I	9	5	142	12	56	13	8
600-C-I	11	4	216	15	93	64	14

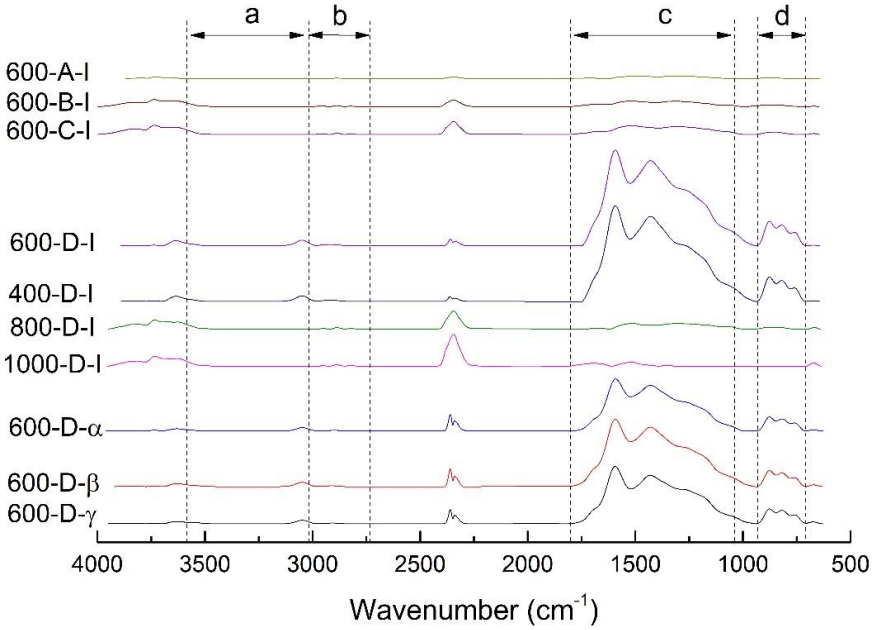

Fig. 3. Infrared spectra of the bio-chars prepared in the different pyrolysis conditions

The oxygen-containing functional groups on the surface of the bio-char promoted the pyrolysis of the biomass (Laurendeau 1978) and were mainly distributed in two vibrational frequency ranges. The frequency range from 1150 to 1350 cm^{-1} mainly corresponded to the stretching vibrations of C-O functional groups, which mainly underwent CO gas devolatilization in the pyrolysis process (Solomon *et al*. 1988). Thus, with an increase in the pyrolysis temperature, the corresponding content of C-O decreased. Furthermore, the relevant contents of ether and ester structures decreased. When the temperature was more than 800 °C, the vibration of the C-O groups disappeared completely. The frequency range near 1600 cm^{-1} belonged to the C=C functional groups of the aromatic nucleus. The aromatic carbon skeleton formed the main structure of the biomass molecule (de la Puente *et al*. 1998) and could undergo polymerization during pyrolysis (Arenillas *et al*. 2004). Therefore, the content of C=C functional groups decreased gradually with an increase in the pyrolysis temperature.

Additionally, the frequency range from 1000 to 1100 cm^{-1} mainly corresponded to the vibrations of Si-O functional groups in the silicate minerals. The content decreased gradually with an increase in the temperature. When the temperature was 800 °C and 1000 °C, the relevant functional groups disappeared. This was because the silicate structure changed, which was caused by high temperatures. This was consistent with the results given previously.

With a decrease in the particle size, the functional group content tended to increase overall. The process of ultrafine particle fragmentation was not only a physical process, but also a chemical one (Palaniandy *et al*. 2008). This was explained by the process of fragmentation, which was accompanied by mechanochemical effects by which the mechanical force might have influenced or induced chemical reactions. In the biomass grinding process using a crusher, when the mechanical force fractures the biomass, the intermolecular forces are destroyed, transforming the biomass from a macromolecular structure into a small molecular structure. Conversely, according to the law of conservation of energy, most of the mechanical energy transmitted to the biomass by the crusher was converted into biomass internal energy, which results in a decreased biomass activation energy.

At the same time, the material surface temperature increases on a macroscopic level. As activated chemical bonds began to occur in the decomposition reaction, new free radicals and functional groups (such as C-O, C=C, COOH, and C=O) are generated. In addition, as the degree of biomass fragmentation increases, the particle size of the biomass decreases, increasing the number of surface functional groups, which is conducive to mercury adsorption. Combined with the previous results, this mechanochemical effect had a certain selectivity and led to more remarkable effects on the oxygen-containing functional groups. Additionally, the pyrolysis area increased with a decrease in the particle size, which affected the contents of the functional groups.

Surface Morphologies of the Bio-chars

The surface morphologies and microstructure characteristics of the bio-chars were obtained with a SEM and are shown in Fig. 4. Because of the effect of the shear stress during the process of fragmentation, the surfaces of the bio-chars became rougher during the process of pyrolysis with a decrease in the particle size. More new pore structures were generated and developed, and a large number of sheet salient structures appeared. The surface morphologies of the bio-chars prepared at the different pyrolysis temperatures were different.

The surface of the 400-D-I sorbent was smooth overall, without holes. The pores formed on the 600-D-I sorbent were deeper and developed. The segmental pores of the 800-D-I sorbent were blocked by tar in a semi-devolatilized state, and the surface was smoother than that of the 600-D-I sorbent. There was no blocking phenomenon seen in the pores of the 1000-D-I sorbent. However, the pore holes were obviously enlarged because of the collapse of the pore structure, ablation of the pore walls, and coalescence of small pores.

Among the sorbents obtained at different heating rates, the surface of the 600-D-α sorbent was smoother, while the pore structures of the 600-D-γ sorbent were developed. The above results verified the conclusions that were drawn previously.

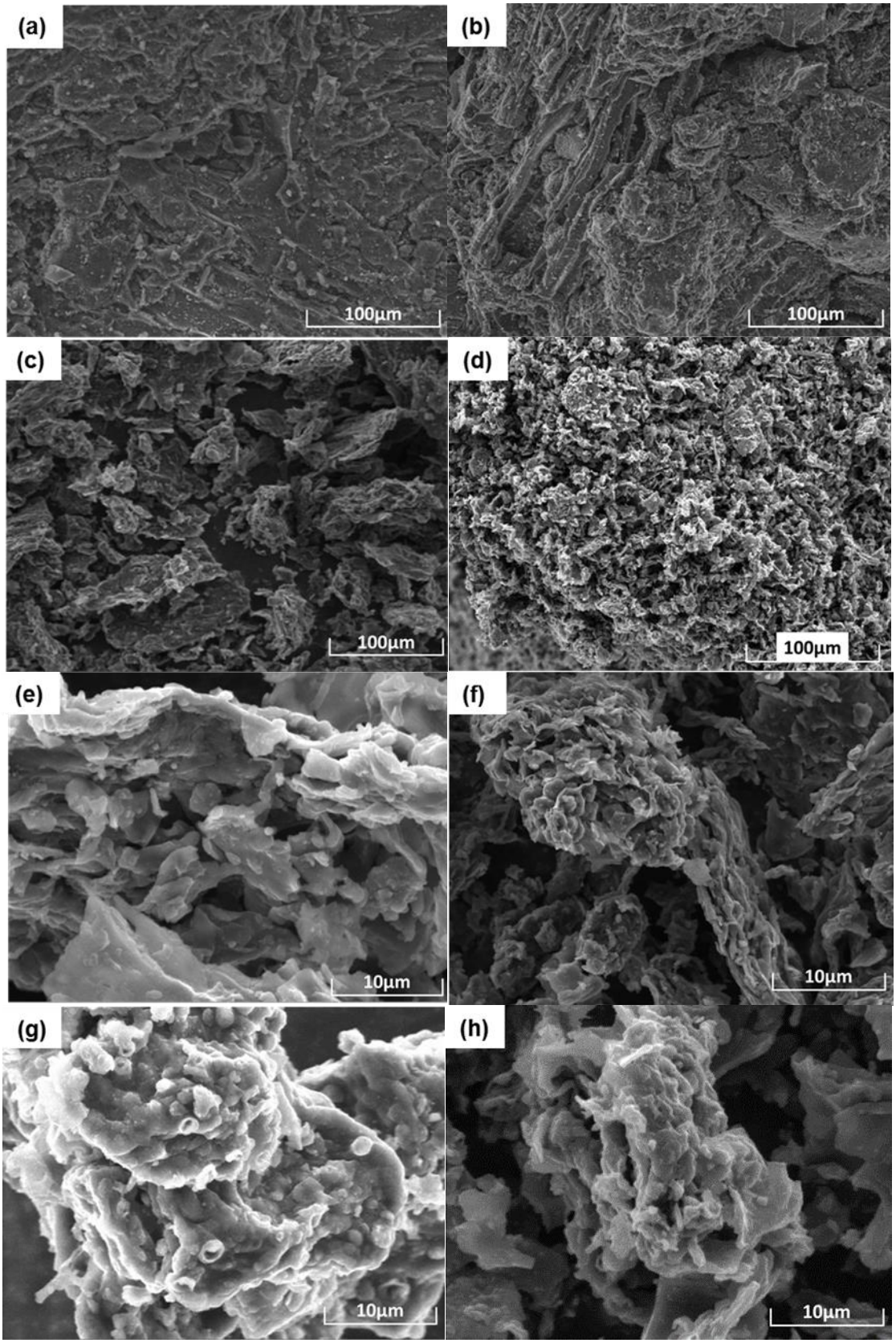
(a)
100μm
(b)
100μm
(c)
100μm
(d)
100μm
(e)
10μm
(f)
10μm
(g)
10μm
(h)
10μm

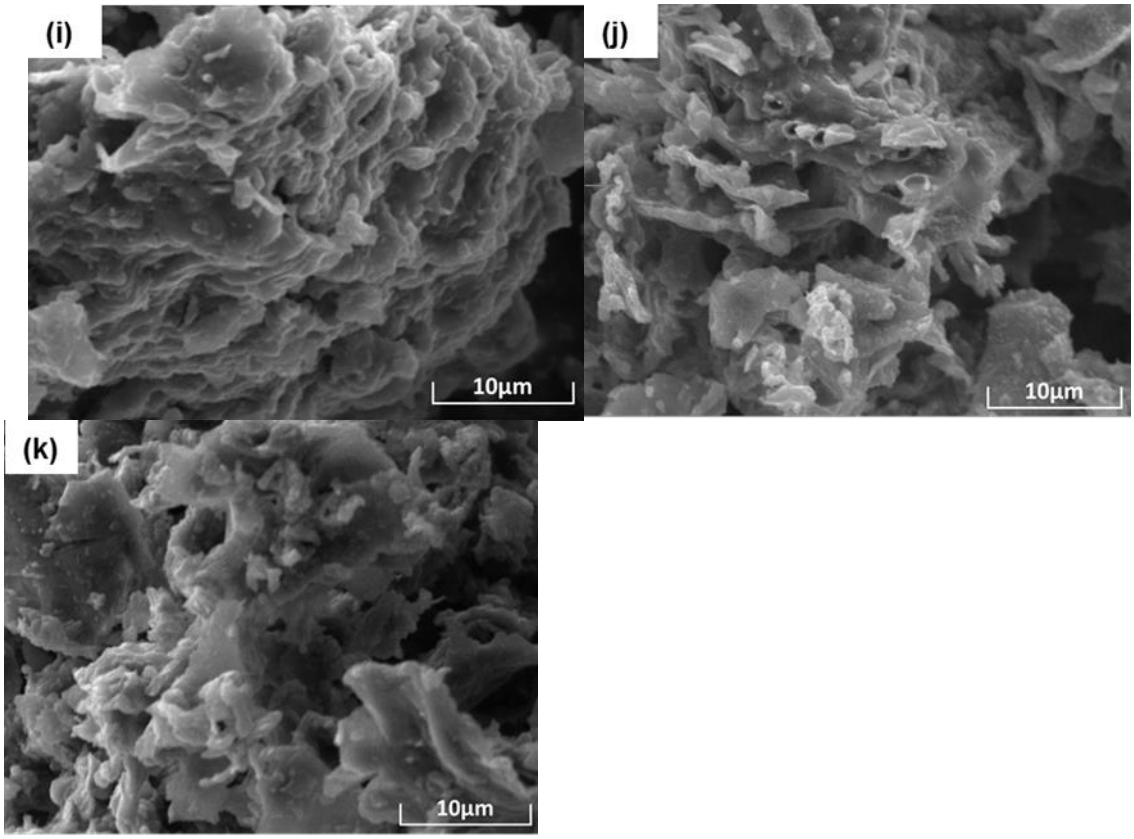

Fig. 4. SEM images of the bio-chars produced under different pyrolysis modes and with different particle sizes: (a) 600-A-I; (b) 600-B-I; (c) 600-C-I; (d) 600-D-I; (e) 400-D-I; (f) 600-D-I; (g) 800-D-I; (h) 1000-D-I; (i) 600-D-α; (j) 600-D-β; and (k) 600-D-γ

Mercury Adsorption Characteristics of the Bio-chars

The mercury adsorption characteristics of the bio-chars prepared under different pyrolysis modes and with different particle sizes are shown in Fig. 5. For the same adsorption conditions and particle size and with an increase in the stationary pyrolysis temperature in the isothermal mode and the final pyrolysis temperature in the non-isothermal mode, the mercury adsorption capacities of the bio-chars initially increased and then decreased. The temperature that corresponded to the highest mercury adsorption capacity was 600 °C, followed by 800 °C, 1000 °C, and 400 °C. The adsorption of mercury by bio-char is dependent upon not only the pore structures, but also the surface chemical properties (Zhai *et al*. 2006; Hu *et al*. 2008). Although the functional groups content of the 400-D-I sorbent was higher, the pore structure parameters were significantly lower, which negatively impacted the adsorption of mercury. Similarly, for the 800-D-I sorbent, although the specific surface area and accumulated pore volume were lower than those of the 1000-D-I sorbent, the functional groups contents were much higher, especially the oxygen-containing functional groups, such as COOH and C=O. Thus, the adsorption capacity of 800-D-I sorbent was better. When 600 °C was the stationary and final temperatures for the different pyrolysis modes, the Hg^0 adsorption capacities were noticeably better than those of the bio-chars that were obtained at the other temperatures. The best mercury removal performance was obtained with the 600-D-I sorbent, for which the mercury penetration coefficient was only 75% when the adsorption time was 19705 s. As mentioned above, the pore structures of the 600-D-I sorbent were substantially larger than those of the sorbents

produced in the other pyrolysis conditions. In addition, a large number of relevant functional groups were formed in the 600-D-I sorbent, which was beneficial for mercury adsorption.

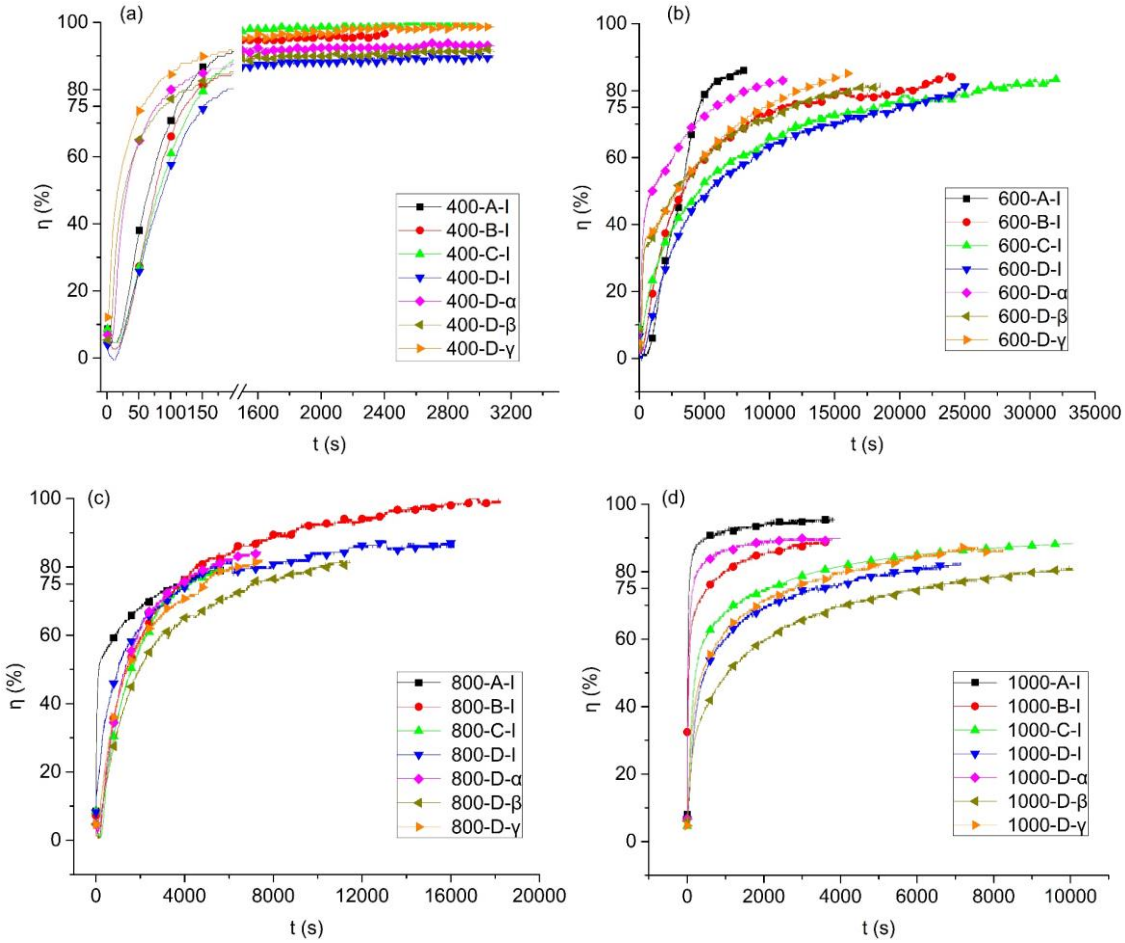

Fig. 5. Mercury adsorption characteristics of the bio-chars produced under different pyrolysis modes and with different particle sizes: (a) 400 °C; (b) 600 °C; (c) 800 °C; and (d) 1000 °C

When the stationary and final temperatures were 600 °C and with a decrease in the particle size, the mercury adsorption capacities of the bio-char sorbents showed a gentle increasing trend overall. The mercury penetration rates of the 600-A-I, 600-B-I, 600-C-I, and 600-D-I sorbents reached 75%, and the corresponding adsorption times were 4580 s, 10630 s, 17780 s, and 19700 s, respectively. For the adsorption time of 8260 s, the q values of these adsorbents were 1293 ng/g, 1480 ng/g, 1620 ng/g, and 1770 ng/g, and the corresponding η values were 86.09%, 69.33%, 60.67%, and 58.67%, respectively. The main reason for this difference was that the functional group contents and pore structure parameters of the bio-chars tended to increase overall, with a decrease in the particle size.

For the bio-chars prepared under the non-isothermal mode, the mercury adsorption capacities of the bio-chars initially increased and then decreased with an increase in the heating rate. The Hg^0 adsorption capacities of the bio-chars obtained with a heating rate of 10 °C/min were the highest. Of these bio-chars, the mercury removal performance of the 600-D-β sorbent was the best. This sorbent had a mercury penetration coefficient of 75% and the corresponding adsorption time was 11750 s. Meanwhile, the adsorption capacities of the sorbents produced at a heating rate of 5 °C/min were lower compared with the

sorbents produced at a 15 °C/min heating rate. This was because that during the process of non-isothermal pyrolysis, compared with the sorbents produced at the other heating rates, the functional groups contents of the sorbents produced at 10 °C/min were higher, which was caused by the optimum pyrolysis temperature range and enhanced the mercury adsorption capacity. And the pyrolysis process of the 600-D-α sorbent mainly occurred in the high-temperature region, which was not conducive to the development of the pore structure and the formation of surface functional groups. However, the adsorption capacity of the 400-D-α sorbent was higher than that of the 400-D-γ sorbent. This could be explained by the poor pore structure of the 400-D-γ sorbent, caused by the fact that the pyrolysis process mainly occurred in the low-temperature region, which was unfavorable for the devolatilization of the volatile compounds and development of the pore structure. Additionally, the mercury removal performances of the sorbents obtained under the non-isothermal preparation condition were inferior overall to those of the sorbents obtained under the isothermal preparation condition. This might be related to the higher functional groups contents of the latter. The adsorption capacities of the 800-D-β, 800-D-γ, and 1000-D-β sorbents were stronger than the sorbents obtained at the corresponding stationary temperatures under the isothermal preparation condition. As mentioned above, the pyrolysis process of these sorbents obtained under the isothermal preparation condition mainly occurred over 800 °C, and so the relative pore volume of the macropores was higher, which was unfavorable for the adsorption of mercury.

Kinetics and Activation Energy of Elemental Mercury Adsorption on the Bio-chars Surface

The adsorption of mercury on bio-char mainly involves three basic steps, which are external mass transfer, surface adsorption, and intraparticle diffusion. In this paper, the pseudo-first-order kinetic model (Eq. 5), pseudo-second-order kinetic model (Eq. 6), intraparticle diffusion model (Eq. 7), and Elovich model (Eq. 8) were used to elucidate the reaction mechanism and determine the rate-limiting step of the adsorption process (Jia *et al*. 2018). The pseudo-first-order relationship can be expresses as follows:

$$q=q_e(1-exp(-tk_1)) \quad (5)$$

In this equation, q is the total amount of mercury adsorbed per unit mass of bio-char at time t (ng/g), q_e is the amount of mercury adsorbed per unit mass of bio-char at equilibrium (ng/g), t is the adsorption time (min), and k_1 is the pseudo-first-order rate constant (min^{-1}).

The pseudo-second-order rate equation is as follows:

$$q=(q_e^2 k_2 t)/(1+q_e k_2 t) \quad (6)$$

In this equation, k_2 is the pseudo-second-order rate constant (ng/(g · min)).

The intraparticle diffusion relationship can be expressed as follows:

$$q=k_{id}t^{1/2}+C \quad (7)$$

In this equation, k_{id} is the intraparticle diffusion rate constant (ng/(g·$min^{1/2}$)) and C is a constant related to the thickness of the boundary layer (ng/g).

The Elovich relationship can be expressed as follows:

$$q=(1/\beta)\ln(t+t_0)-(1/\beta)\ln(t_0) \quad (8)$$

In this equation, α is the initial adsorption rate (ng/(g·$min^{1/2}$)), β is a constant related to the surface coverage and activation energy (ng/g), and $t_0=1/(\alpha\cdot\beta)$.

The fitting results are shown in Table 5. The coefficients of determination, R^2, of the bio-char sorbents were all close to 0.99, indicating that the adsorption processes of the bio-char sorbents prepared under different conditions were consistent with these four kinetic models. The adsorption processes were affected by both physical adsorption and chemical adsorption. In addition, mercury adsorption was related to the adsorption sites of the bio-char rather than monolayer adsorption.

Although the rate constants of the pseudo-first-order and pseudo-second-order models for the 1000-D-I sorbent were lower than those of the other sorbents, based on the discussion above, this difference was mainly due to the poor surface pore structure and low content of functional groups in the 1000-D-I sorbent. In addition, for the 600-D-α, 600-D-β, and 600-D-γ sorbents, the rate-limiting steps were mainly chemical adsorption.

Moreover, k_{id} increased with decreasing particle size. And the k_{id} of 600-D-I sorbent was much larger than that of the other bio-char sorbents. This difference mainly occurred because the pore richness Z of the former sorbent was larger than those of the latter, indicating the presence of more abundant pores, which facilitated the diffusion of mercury in the particles. Meanwhile, the R^2 values obtained for the intraparticle diffusion model were lower than those obtained for the pseudo-first-order kinetic model. Thus, external mass transfer rather than internal diffusion was judged to be the rate-limiting step of mercury adsorption on the surface of the bio-char.

The fitting of the Elovich kinetic model matched well with the experimental results. Thus, the occurrence of chemical adsorption by the active sites was verified. In addition, the initial mercury adsorption rate, α, increased with increasing content of surface functional groups in the bio-char sorbent.

The adsorption activation energy (E_a) represents the energy required by the adsorbate molecules to reach an active state before adsorption. Generally, E_a values in the range of 0 to -4 kJ/mol represent physical adsorption, and -40 to -800 kJ/mol represents chemical adsorption. The adsorption activation energy is obtained by the Arrhenius equation (Eq. 9),

$$lnk_2 = -\frac{E_a}{RT} + lnk_0 \quad (9)$$

where E_a is the adsorption activation energy (kJ/mol), R is the gas constant (equal to 8.314 J/(mol·K)), T is the flue gas temperature (K), and k_0 is the temperature impact factor.

Figure 6 is the result of the linear fitting of mercury adsorption on bio-char sorbents using the Arrhenius equation. Table 6 shows the obtained fitting parameters. The E_a values were in the range of -4 kJ/mol to -40 kJ/mol, indicating that the adsorption of mercury on the surface of bio-char sorbents was a combination of physical adsorption and chemical adsorption. Among them, the E_a value of mercury adsorbed on the 1000-D-I sorbent surface was closest to -4 kJ/mol, demonstrating that the physical adsorption was the main adsorption form. With decreasing particle size, the absolute value of E_a gradually increased, indicating that the adsorption gradually changed from physical adsorption to chemical adsorption. The required activation energy of mercury adsorption on the 600-D-I sorbent surface was more than twice that of mercury adsorbed on the 600-A-I sorbent surface, indicating that the adsorption of mercury on the 600-D-I sorbent surface required more energy, mainly due to the strengthening of chemical adsorption. These results are consistent with previous research conclusions.

Table 5. The Fitting Parameters of the Bio-chars

Sorbents	Pseudo-first order kinetic			Pseudo-second order kinetic		
	R^2	k_1	q_e	R^2	k_2	q_e
400-D-I	0.9721	6.21×10^{-5}	89	0.9829	1.33×10^{-6}	113
600-D-I	0.9956	1.46×10^{-3}	5325	0.9993	1.95×10^{-7}	8019
800-D-I	0.9997	8.54×10^{-5}	3944	0.9992	1.48×10^{-8}	6266
1000-D-I	0.9999	1.94×10^{-5}	964	0.9998	8.81×10^{-10}	1498
600-D-α	0.9989	1.18×10^{-4}	1598	0.9992	2.63×10^{-8}	2669
600-D-β	0.9989	1.31×10^{-4}	2663	0.9996	3.08×10^{-8}	4055
600-D-γ	0.9999	1.33×10^{-4}	1950	0.9999	1.85×10^{-7}	3315
600-A-I	0.9998	7.04×10^{-5}	955	0.9987	6.26×10^{-9}	1396
600-B-I	0.9997	2.45×10^{-4}	1073	0.9961	6.63×10^{-9}	1328
600-C-I	0.9974	3.45×10^{-4}	2377	0.9991	2.38×10^{-8}	3441

Sorbents	Intra-particle diffusion			Elovich kinetic		
	R^2	k_{id}	c	R^2	α	β
400-D-I	0.9718	1.78	7	0.9933	0.5365	3.44×10^{-2}
600-D-I	0.9907	33.21	-683	0.9999	0.4387	3.49×10^{-4}
800-D-I	0.9989	12.74	-535	0.9956	0.2638	4.21×10^{-4}
1000-D-I	0.9998	10.01	-119	0.9948	0.2118	1.79×10^{-3}
600-D-α	0.9872	13.69	-203	0.9994	0.2720	9.17×10^{-4}
600-D-β	0.9976	16.59	-330	0.9999	0.3541	6.80×10^{-4}
600-D-γ	0.9868	18.25	-254	0.9999	0.4058	7.20×10^{-4}
600-A-I	0.9997	7.91	-102	0.9405	0.2259	2.09×10^{-3}
600-B-I	0.9976	18.3	-126	0.9914	0.2563	3.02×10^{-3}
600-C-I	0.9949	23.6	-226	0.9999	0.2673	8.65×10^{-4}

Table 6. Arrhenius Equation Fitting Parameters

	400-D-I	600-D-I	800-D-I	1000-D-I	600-D-α	600-D-β	600-D-γ	600-A-I	600-B-I	600-C-I
E_a (kJ/mol)	-35.9	-31.67	-15.55	-10.14	-27.68	-29.29	-29.44	-12.95	-17.51	-27.67
R^2	0.8671	0.8725	0.8872	0.8714	0.8847	0.8726	0.8996	0.8958	0.8737	0.8890

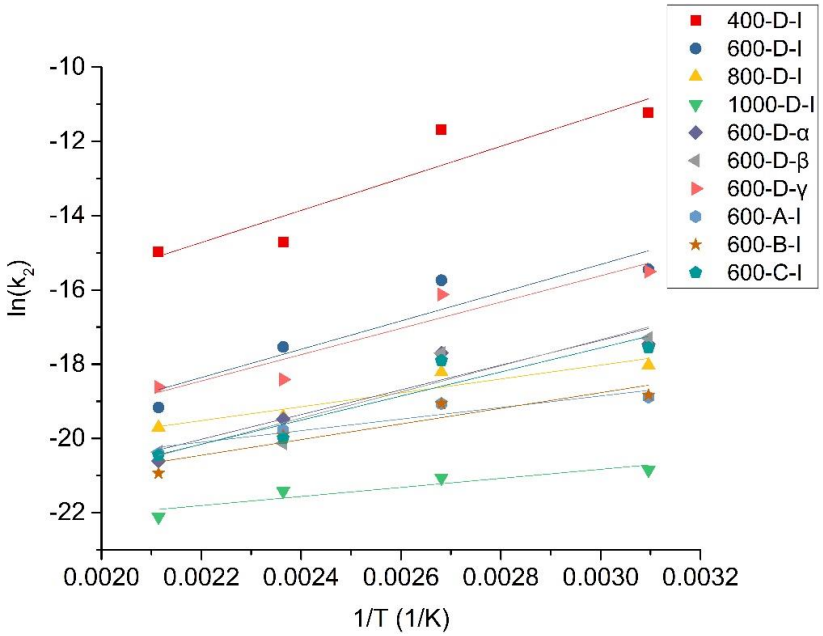

Fig. 6. Linear fitting of Hg adsorption on the bio-char sorbents surface by the Arrhenius equation

CONCLUSIONS

1. The processes of WS biomass pyrolysis could be divided into three stages. The biomass with the smaller particle size had the larger reaction area, weakening the influence of mass transfer and heat transfer on the pyrolysis process, which was beneficial to the progress of the pyrolysis and the devolatilization of the volatiles. The heating rate played a more important role in the pyrolysis of the biomass than the particle size, in the experimental conditions analyzed.
2. Differences were observed in the mercury adsorption characteristics of bio-chars prepared in various pyrolysis conditions. The temperature that corresponded to the best mercury adsorption capacity was 600 °C, followed by 800 °C, 1000 °C, and 400 °C. With the decrease in the particle size, the mercury adsorption capacity of the bio-char sorbents showed an overall gradually increasing trend. The main reason for this difference was that the functional group contents and pore structure parameters of the bio-chars tended to increase overall. The Hg^0 adsorption capacities of the bio-char sorbents obtained with a heating rate of 10 °C/min were better. This was related to the higher functional groups contents. Among the examined bio-chars, the 600-D-I sorbent had the highest adsorption capacity. The pore structures of this sorbent were substantially larger than those of the sorbents produced in the other pyrolysis conditions. In addition, a large number of relevant functional groups were formed in the 600-D-I sorbent, which was beneficial for mercury adsorption.
3. The mercury adsorption processes were affected by both physical adsorption and chemical adsorption. With the increase in the pyrolysis temperature, the R^2 value calculated for the pseudo-first-order kinetic model became closer to that of the pseudo-second-order kinetic model. Furthermore, the rate constants of the pseudo-first-order and pseudo-second-order models gradually increased, with decreasing particle size. In addition, mercury adsorption was related to the adsorption sites of the bio-char rather than monolayer adsorption.

ACKNOWLEDGEMENTS

The authors acknowledge the financial support of this work provided by the National Natural Science Foundation of China (Grant No. U1510135) and the Science and Technology Major Projects of Shanxi Province (Grant No. MD2015-04).

We thank Shelley C. Barry, PhD for the linguistic assistance during the preparation of this manuscript.

REFERENCES CITED

Antal, M. J., and Varhegyi, G. (1995). "Cellulose pyrolysis kinetics: The current state of knowledge," *Ind. Eng. Chem. Res.* 34(3), 703-717. DOI: 10.1021/ie00042a001

Arenillas, A., Pevida, C., Rubiera, F., García, R., and Pis, J. J. (2004). "Characterisation of model compounds and a synthetic coal by TG/MS/FTIR to represent the pyrolysis behaviour of coal," *J. Anal. Appl. Pyrol.* 71(2), 747-763. DOI: 10.1016/j.jaap.2003.10.005

ASTM E1756-08 (2015). "Standard test method for determination of total solids in biomass," ASTM International, West Conshohocken, PA.

Babu, B. V., and Sheth, P. N. (2006). "Modeling and simulation of reduction zone of downdraft biomass gasifier: Effect of char reactivity factor," *Energ. Convers. Manage.* 47(15-16), 2602-2611. DOI: 10.1016/j.enconman.2005.10.032

Becidan, M., Skreiberg, Ø., and Hustad, J. E. (2007). "Products distribution and gas release in pyrolysis of thermally thick biomass residues samples," *J. Anal. Appl. Pyrol.* 78(1), 207-213. DOI: 10.1016/j.jaap.2006.07.002

Carey, T. R., Hargrove, O. W., Richardson, C. F., Chang, R., and Meserole, F. B. (1998). "Factors affecting mercury control in utility flue gas using activated carbon," *JAPCA J. Air Waste MA* 48(12), 1166-1174. DOI: 10.1080/10473289.1998.10463753

de la Puente, G., Iglesias, M. J., Fuente, E., and Pis, J. J. (1998). "Changes in the structure of coals of different rank due to oxidation - Effects on pyrolysis behavior," *J. Anal. Appl. Pyrol.* 47(47), 33-42. DOI: 10.1016/S0165-2370(98)00087-4

Duan, J., Luo, Y.-h., Lu, F., Chen, Y., Hu, L.-y., and Wang, Q.-c. (2006). "Thermogravimetric analysis of pyrolysis characteristics of biomass wastes," *Industrial Heating* 35(3), 10-13.

Fan, B., Jia, L., Li, X., Liu, J., Zheng, X., and Jin, Y. (2016). "Study on mercury adsorption by fly ash from coal-fired boilers of power plants," *Journal of Chinese Society of Power Engineering* 36(8), 621-628.

Fu, P., Yi, W., Bai, X., Li, Z., Hu, S., and Xiang, J. (2011). "Effect of temperature on gas composition and char structural features of pyrolyzed agricultural residues," *Bioresource Technol.* 102(17), 8211-8219. DOI: 10.1016/j.biortech.2011.05.083

Fuente-Cuesta, A., Diaz-Somoano, M., Lopez-Anton, M. A., Cieplik, M., Fierro, J. L., and Martínez-Tarazona, M. R. (2012). "Biomass gasification chars for mercury capture from a simulated flue gas of coal combustion," *J. Environ. Manage.* 98, 23-28. DOI: 10.1016/j.jenvman.2011.12.013

GB 13223-2011 (2012). "Emission standard of air pollutants for thermal power plants," Standardization Administration of China, Beijing, China.

Gbor, P. K., Wen, D., Meng, F., Yang, F., Zhang, B., and Soloan, J. J. (2006). "Improved model for mercury emission, transport and deposition," *Atmos. Environ.* 40(5), 973-983. DOI: 10.1016/j.atmosenv.2005.10.040

Graydon, J. W., Zhang, X., Kirk, D. W., and Jia, C. Q. (2009). "Sorption and stability of mercury on activated carbon for emission control," *J. Hazard. Mater.* 168(2-3), 978-982. DOI: 10.1016/j.jhazmat.2009.02.118

Hu, S., Xiang, J., Sun, L., Xu, M., Qiu, J., and Fu, P. (2008). "Characterization of char from rapid pyrolysis of rice husk," *Fuel Process. Technol.* 89(11), 1096-1105. DOI: 10.1016/j.fuproc.2008.05.001

Ibarra, J., Muñoz, E., and Moliner, R. (1996). "FTIR study of the evolution of coal structure during the coalification process," *Org. Geochem.* 24(6-7), 725-735. DOI: 10.1016/0146-6380(96)00063-0

Jarzębski, A. B., Lorenc, J., Aristov, Y. I., and Lisitza, N. (1995). "Porous texture characteristics of a homologous series of base-catalyzed silica aerogels," *J. Non-Cryst. Solids* 190(3), 198-205. DOI: 10.1016/0022-3093(95)00276-6

Jia, L., Fan, B., Huo, R., Li, B., Yao, Y., Han, F., Qiao, X., and Jin, Y. (2018a). "Study on quenching hydration reaction kinetics and desulfurization characteristics of magnesium slag," *J. Clean. Prod.* 190, 12-23. DOI: 10.1016/j.jclepro.2018.04.150

Jia, L., Li, B., Xu, L., Zheng, X., Qiao, X., and Fan, B. (2018b). "Effects of different preparation conditions on kinetics and adsorption of mercury by biomass char," *J. Chinese Journal of Environmental Engineering* 12, 134-144. DOI: 10. 12030/j. cjee. 201706018

Keown, D. M., Hayashi, J.-I., and Li, C.-Z. (2008). "Drastic changes in biomass char structure and reactivity upon contact with steam," *Fuel* 87(7), 1127-1132. DOI: 10.1016/j.fuel.2007.05.057

Keown, D. M., Li, X., Hayashi, J.-I., and Li, C.-Z. (2007). "Characterization of the structural features of char from the pyrolysis of cane trash using Fourier transform-Raman spectroscopy," *Energ. Fuel.* 21(3), 1816-1821. DOI: 10.1021/ef070049r

Koch, A., Krzton, A., Finqueneisel, G., Heintz, O., Weber, J.-V., and Zimny, T. (1998). "A study of carbonaceous char oxidation in air by semi-quantitative FTIR spectroscopy," *Fuel* 77(6), 563-569. DOI: 10.1016/S0016-2361(97)00157-9

Laurendeau, N. M. (1978). "Heterogeneous kinetics of coal char gasification and combustion," *Prog. Energ. Combust.* 4(4), 221-270. DOI: 10.1016/0360-1285(78)90008-4

Ma, Z., Chen, D., Gu, J., Bao, B., and Zhang, Q. (2015). "Determination of pyrolysis characteristics and kinetics of palm kernel shell using TGA-FTIR and model-free integral methods," *Energ. Convers. Manage.* 89, 251-259. DOI: 10.1016/j.enconman.2014.09.074

Newalkar, G., Iisa, K., D'Amico, A. D., Sievers, C., and Agrawal, P. (2014). "Effect of temperature, pressure, and residence time on pyrolysis of pine in an entrained flow reactor," *Energ. Fuel.* 28(8), 5144-5157. DOI: 10.1021/ef5009715

Palaniandy, S., Azizli, K. A. M., Hussin, H., and Hashim, S. F. S. (2008). "Mechanochemistry of silica on jet milling," *J. Mater. Process. Tech.* 205(1-3), 119-127. DOI: 10.1016/j.jmatprotec.2007.11.086

Park, H. J., Park, S. H., Sohn, J. M., Park, J., Jeon, J.-K., Kim, S.-S., and Park, Y.-K. (2010). "Steam reforming of biomass gasification tar using benzene as a model compound over various Ni supported metal oxide catalysts," *Bioresource Technol.* 101(1), S101-S103. DOI: 10.1016/j.biortech.2009.03.036

Pfeifer, P. (1988). "Fractals in surface science: Scattering and thermodynamics of adsorbed films," in: *Chemistry and Physics of Solid Surfaces VII*, R. Vanselow and R. Howe (eds.), Springer Berlin Heidelberg, Berlin, Germany, pp. 283-305.

Pisupati, S. V., and Bhallaa, S. (2008). "Numerical modeling of NO_x reduction using pyrolysis products from biomass-based materials," *Biomass Bioenerg.* 32(2), 146-154. DOI: 10.1016/j.biombioe.2007.07.010

Sanchez-Silva, L., López-González, D., Villaseñor, J., Sánchezet, P., and Valverde, J. L. (2012). "Thermogravimetric-mass spectrometric analysis of lignocellulosic and marine biomass pyrolysis," *Bioresource Technol.* 109, 163-172. DOI: 10.1016/j.biortech.2012.01.001

Senneca, O. (2007). "Kinetics of pyrolysis, combustion and gasification of three biomass fuels," *Fuel Process. Technol.* 88(1), 87-97. DOI: 10.1016/j.fuproc.2006.09.002

Solomon, P. R., Hamblen, D. G., Carangelo, R. M., Serio, M. A., and Deshpande, G. V. (1988) "Models of tar formation during coal devolatilization," *Combust. Flame* 71(2), 137-146. DOI: 10.1016/0010-2180(88)90003-X

Syversen, T., and Kaur, P. (2012). "The toxicology of mercury and its compounds," *J. Trace Elem. Med. Bio.* 26(4), 215-226. DOI: 10.1016/j.jtemb.2012.02.004

Wu, D., Zhang, S., and Zhu, T. (2011). "Controlling mercury emission for China's coal fired electricity plants: An economic analysis," *Enrgy Proced.* 5, 1439-1454. DOI: 10.1016/j.egypro.2011.03.248

Yin, J.-j., Duan, Y.-f., Wang, Y.-j., Wang, H., Mao, Y.-q., and Wei, H.-q. (2012). "Characterization of biomass char and its mercury adsorption performance," *Journal of Fuel Chemistry and Technology* 40, 390-396.

Zeng, H., Feng, J., and Guo, J. (2004). "Removal of elemental mercury from coal combustion flue gas by chloride-impregnated activated carbon," *Fuel* 83(1), 143-146. DOI: 10.1016/S0016-2361(03)00235-7

Zhai, S., Liu, J., Yang, S., Zeng, Y., and Xiao, Y. (2006). "Flue gas purification technology using activated coke and its application prospects in China," *Environmental Protection of Chemical Industry* 26(3), 204-208.

Zhang, B., Luo, G.-Q., Xu, P., Yu, Q., Qiu, Y., Wu, H., and Yao, H. (2015). "Effect of oxygen fictional groups of activated carbon on mercury adsorption," *J. Eng. Thermophys.* 36, 1611-1615.

Zhang, L., and Wong, M. H. (2007). "Environmental mercury contamination in China: Sources and impacts," *Environ. Int.* 33(1), 108-121. DOI: 10.1016/j.envint.2006.06.022

Article submitted: December 13, 2017; Peer review completed: March 11, 2018; Revised version received: May 20, 2018; Accepted: May 22, 2018; Published: May 25, 2018.
DOI: 10.15376/biores.13.3.5450-5471